Electronic Supplementary Information

A Freestanding SiO_2 Ultrathin Membrane with NiCu Nanoparticles Embedding on Its Double-faces for Catalyzing Nitro-amination

Chen Gu†, Dandan Wu†, Ming Wen, and Qingsheng Wu*

School of Chemical Science and Engineering, State Key Laboratory of Pollution Control and Resource Reuse, Shanghai Key Laboratory of Chemical Assessment and Sustainability, Tongji University, Shanghai 200092, P. R. China

Corresponding Authors

*Ming Wen: E-mail: m_wen@tongji.edu.cn.

1. The Supplement of Experimental Section

1.1 Chemicals

Nickel chloride hexahydrate ($NiCl_2 \cdot 6H_2O$, 98%), copper chloride dihydrate ($CuCl_2 \cdot 2H_2O$, 99%), ethanol (C_2H_5OH, 99%), ethanol (C_2H_5OH, 75%) and acetone (C_3H_6O, 99.5%) were purchased from Sinopharm Chemical Reagent Co., Ltd. (SCRC). Sodium borohydride ($NaBH_4$, 98%), urea (CH_4N_2O, 99%) and 4-nitrophenol (4-NP), 4-aminophenol (4-AP), 4-nitroanisole, 4-anisidine, 4-nitrobenzyl alcohol, 4-aminobenzyl alcohol, 4-nitrobenzaldehyde, 4-aminobenzaldehyde, 4-nitrotoluene and 4-toluidine were purchased from Aladdin Reagents, Shanghai. All reagents were used without further purification. The silicon wafers were purchased from Zhejiang Lijing Silicon Material Co., Ltd. and they were used after pretreatment.

1.2 Pretreatment of silicon wafers

The silicon wafers were cut into small pieces of 5mm*5mm. Then the small pieces of silicon wafers were alternately washed by ethanol and acetone until the solution is no longer turbid. After that, they were washed by deionized water for three times and kept in deionized water for further experiments.

2. Results and Discussion

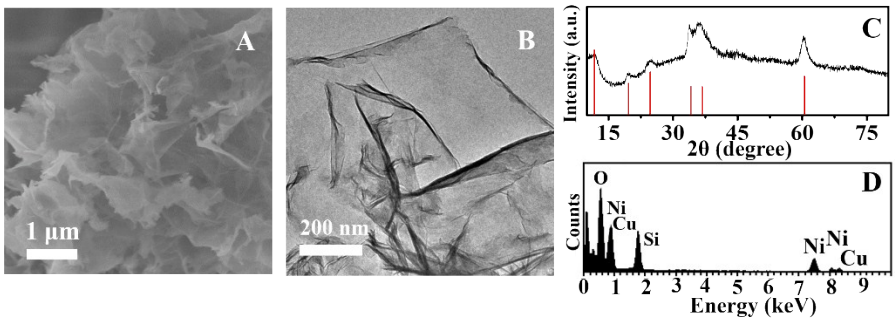

Figure S1. SEM (A), TEM (B) images, XRD pattern (C) and EDS analysis (D) of NiCu-SiO_2 nanocomposite precursor.

Figure S1 shows the morphology characterization and structure analysis of NiCu-SiO_2 nanocomposite precursor. By SEM and TEM images (Figure 1A, B), a freestanding ultrathin membrane can be observed. The XRD pattern (Figure S1C) shows six peaks and all the diffraction peaks (12.0° (002), 19.5° (110) and 24.4° (004), 34.1° (200), 36.7° (202) and 60.5° (060)) match well with the standard pattern of $Ni_3Si_2O_5(OH)_4$, whereas EDS analysis of the nanocomposite in Figure 1D shows it contains Cu element, therefore NiCu-SiO_2 nanocomposite precursor could be named as $NiCuSiO_3$-hydroxide.

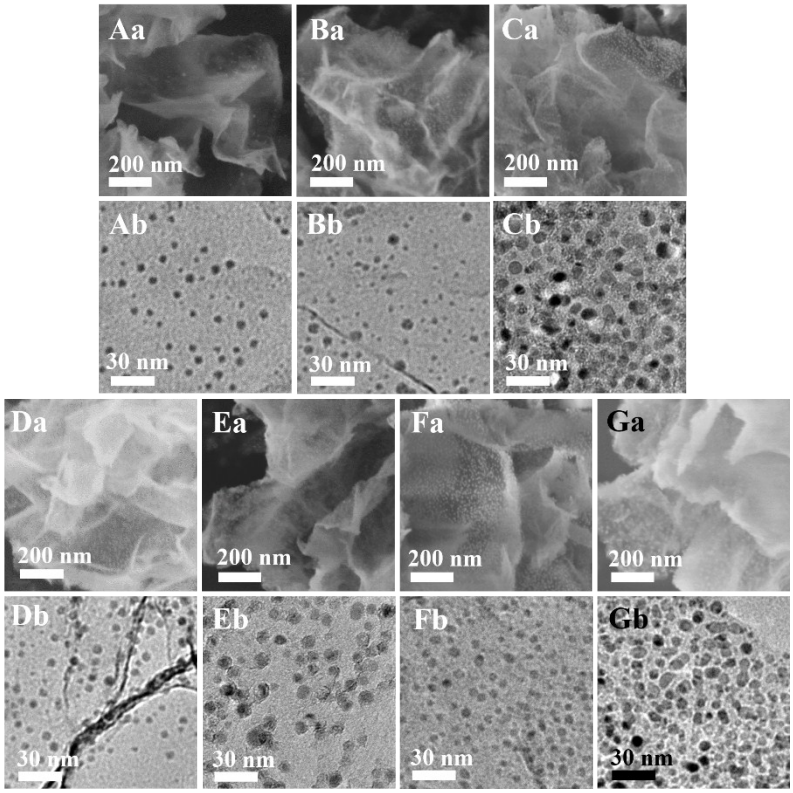

Figure S2. SEM images (a) and TEM images (b) of NiCu-SiO_2 nanocomposite obtained by different reducing conditions: 500°C for 2 h (A), 600°C for 2 h (B), 700°C for 2 h (C), 500°C for 5 h (D), 500°C for 8 h (E), 600°C for 5 h (F) and 600°C for 8 h (G).

In order to obtain 2D structured NiCu-SiO_2 nanocomposite with uniform distribution of NiCu alloy NPs, different reducing conditions have been studied in detail. Firstly, 500 °C for 2 h, 600 °C for 2 h and 700 °C for 2 h reducing conditions have been designed and performed. From Figure S2A~2C, we can clearly see that the high temperature (700 °C) make the size of NiCu alloy NPs increased quickly. And then the different reducing time for 500 °C and 600 °C have been further performed, as shown in Figure S2D~2G, we can observe that the size of NiCu alloy NPs increased with the reducing time such as 500°C for 8 h and 600°C for 8 h, meanwhile, the precursor can't be completely reduced at 500°C. From the above, 600°C for 5 h can be the optimum reducing conditions.

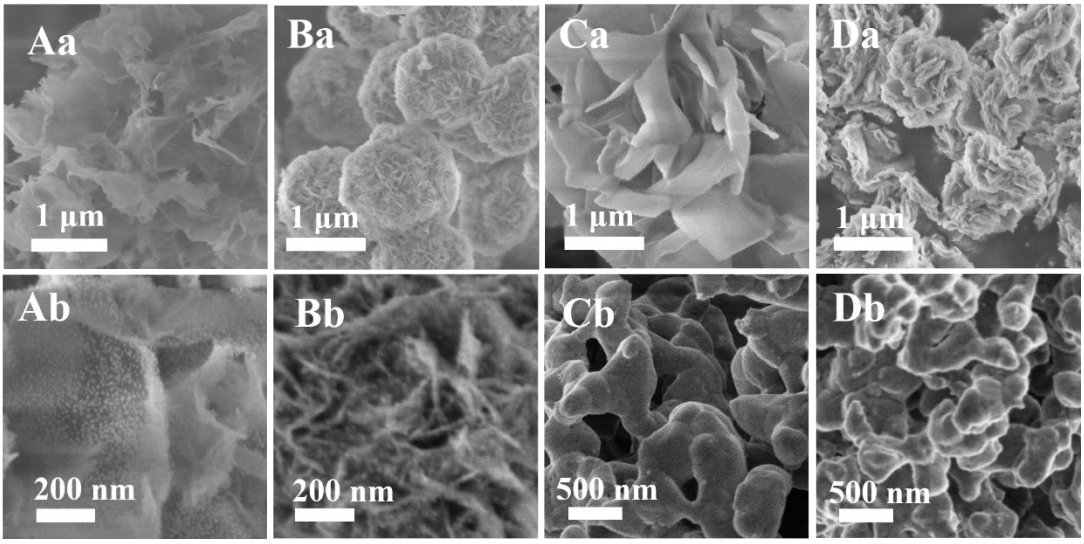

Figure S3. SEM images of the precursor of NiCu-SiO_2 nanocomposite (A), Ni-SiO_2 nanocomposite (B), NiCu (C) and Ni (D) before (a) and after (b) H_2 reduction at 600℃ for 5 h.

As shown in Figure S3A, $NiCuSiO_3$-hydroxide precursor could be reduced under high temperature to obtain 2D structured NiCu-SiO_2 nanocomposite with NiCu NPs evenly embedding on SiO_2 nanosheets. Additionally, Figure S3B presents $NiSiO_3$-hydroxide precursor can also be reduced to Ni-SiO_2 nanocomposite and maintained the original 2D structure, proving the morphology thermal stability may be ascribed to the presence of SiO_2. From Figure S3C and Figure S3D, we can clearly see that the reduced products without the protection of SiO_2 have obvious aggregation, further confirming the above conclusion.

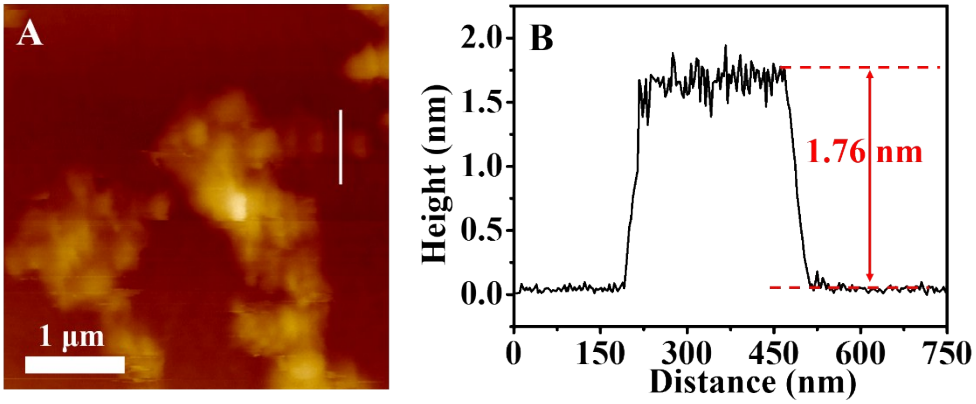

Figure S4. AFM image of SiO_2 membrane prepared by etching the NiCu of NiCu-SiO_2 nanocomposite (A) and height profile of SiO_2 nanosheets (B).

To further confirm the thickness of SiO_2 membrane, AFM and corresponding height profile were performed, as shown in Figure S4B, the SiO_2 membrane have a height of 1.76 nm, which is consistent with the thickness presented in the high-magnification TEM image (Figure 1H).

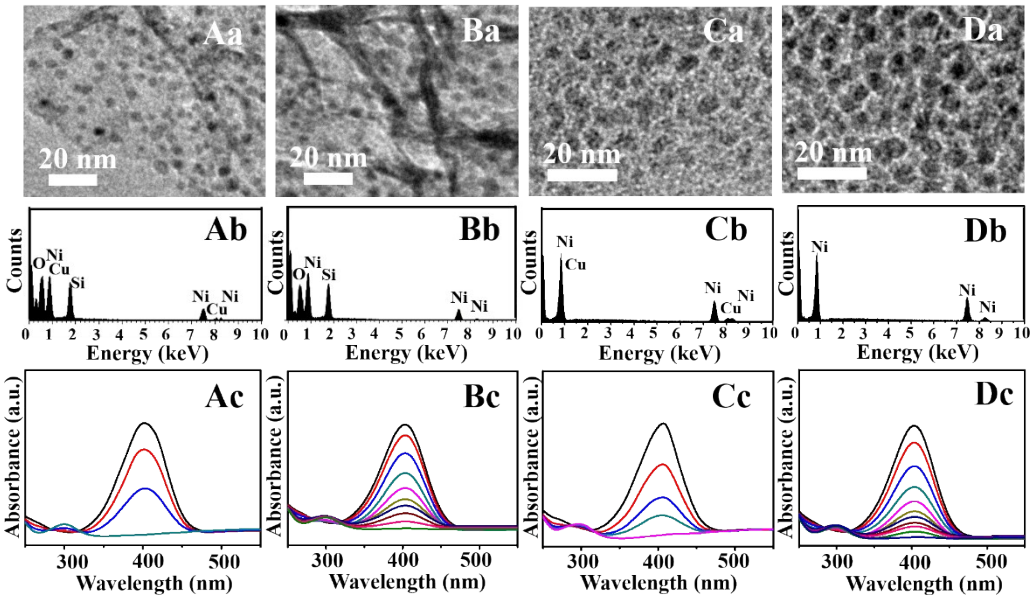

Figure S5. (a) TEM images, (b) EDS analysis and (c) UV-Vis spectra of different catalysts: (A) NiCu-SiO_2 nanocomposite; (B) Ni-SiO_2 nanocomposite; (C) NiCu NPs and (D) Ni NPs.

The morphology characterization and element analysis of Ni-SiO_2 nanocomposite, NiCu NPs and Ni NPs are also presented in Figure S5. In the TEM image of Ni-SiO_2 nanocomposite we can clearly observe that Ni NPs evenly distribute on the double-surfaces of SiO_2 support. And both of the obtained NiCu NPs and Ni NPs by etching SiO_2 support of NiCu-SiO_2 and Ni-SiO_2 nanocomposite have an average diameter of 7 nm in a narrow distribution. The EDS analysis of NiCu-SiO_2 and Ni-SiO_2 nanocomposites present Ni, Cu, Si, O and Ni, Si, O elements, respectively; and reveal the molar ratio of Si/Ni/Cu at 20:10:1, which can be confirmed by ICP data. Meanwhile, no Si element can be observed in NiCu NPs and Ni NPs, indicating the complete removement of SiO_2 support.

The UV-Vis adsorption spectra for the nitro-amination reaction of 4-NP catalyzed by NiCu-SiO_2 nanocomposite, Ni-SiO_2 nanocomposite, NiCu NPs and Ni NPs are shown in Figure S5Ac, S5Bc, S5Cc and S5Dc, respectively. It can be clearly seen that the peak of 4-NP for NiCu-SiO_2 nanocomposite decreases much more quickly than others, especially Ni NPs, demonstrating the obvious advantages of the nanocomposite structure and the synergetic effect of alloys.

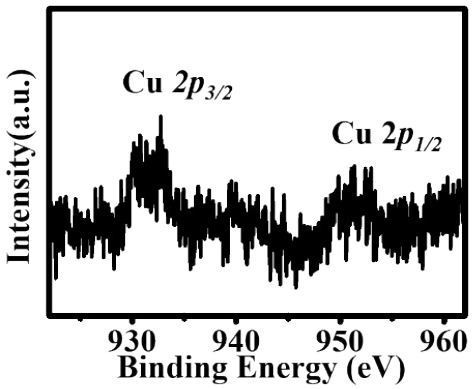

Figure S6. Detailed XPS analysis for Cu 2*p*.

Figure S6 presents the detailed XPS analysis of Cu 2*p*, and the peaks located at the binding energies of 931.2 eV and 951.4 eV are corresponding to the Cu (0), as the nanocomposite only contained a small amount of Cu, the unsmooth spectrum was resulting from great influence of external environment.

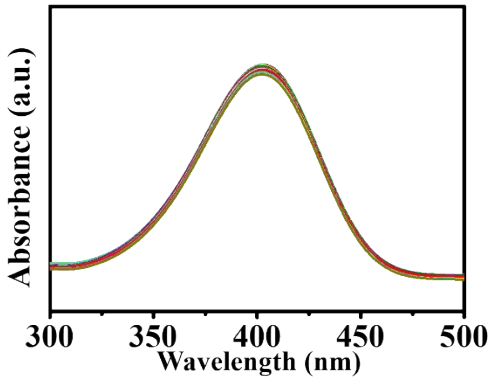

Figure S7. UV-vis spectra for nitro-amination reaction of 4-NP without catalyst.

Figure S7 presents the spectra of blank experiment, which performed the reduction of 4-NP at room temperature and ambient atmosphere by employing excess $NaBH_4$ without any catalysts in the reaction. The absorption peak at 400 nm represents 4-NP, and the peak intensity remains unchanged over time and shows a series of overlapped spectra, indicating the reaction can't take place without catalyst involving in the reaction.

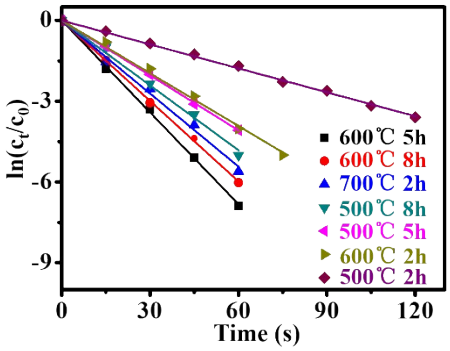

Figure S8. Plots of $\ln(C_t/C_0)$ versus time for the amination reaction of 4-NP catalyzed by NiCu-SiO_2 nanocomposite obtained by different reducing conditions.

Table S1. Comparison of the catalytic performance of NiCu-SiO_2 nanocomposite obtained by different reducing conditions.

Reducing conditions	*k*	No. of cycle
700°C 2h	0.0905	12
600°C 8h	0.0996	13
600°C 5h	0.1138	23
600°C 2h	0.0653	20
500°C 8h	0.0803	15
500°C 5h	0.0680	20
500°C 2h	0.0296	18

Figure S8 and Table S1 present the catalytic performance of NiCu-SiO_2 nanocomposite obtained by different reducing conditions. We found that NiCu-SiO_2 nanocomposite obtained by reducing at 600°C for 5h possesses the best catalytic activity and stability. When reducing condition were 700°C 2h, 600°C 8h and 500°C 8h, NiCu NPs size of NiCu-SiO_2 nanocomposite was bigger than others (Figure S2), which eventually leads to easier aggregation of NiCu NPs and shows worse catalytic stability. In addition, when reduced at 600°C for 2h, 500°C for 5h and 500°C for 2h, especially 500°C for 2h, the rate constants *k* was only 0.0296 which is much lower than others, because only a fraction of NiCu alloy NPs can been obtained, as shown in Figure S2A.

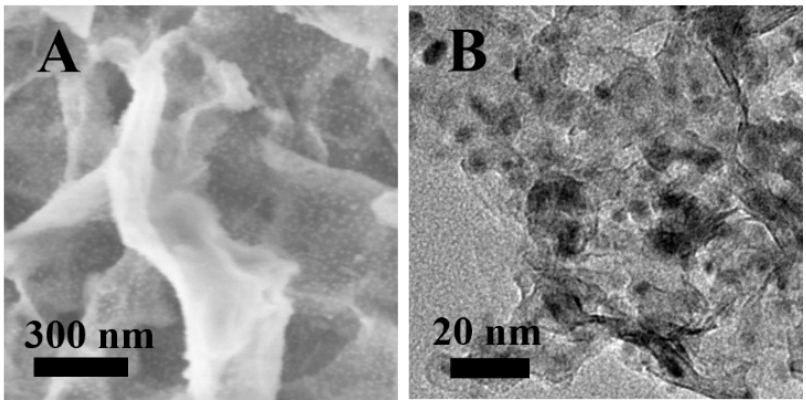

Figure S9. SEM (A) and TEM (B) images of NiCu-SiO_2 nanocomposite after 20 times successive catalytic tests.

The morphology of NiCu-SiO_2 nanocomposite after long-term recycling tests was also monitored and shown in Figure S9. From the SEM image (Figure S9A) we can clearly see that after long-term recyclability tests, the NiCu-SiO_2 nanocomposite still remained 2D structure. However, the TEM image in Figure S9B shows that NiCu NPs were coated by a layer of nanosheets, which explains the slight deactivation of NiCu-SiO_2 nanocomposite after 20 times successive catalytic tests.

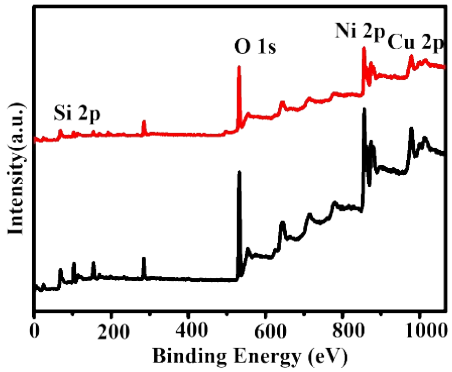

Figure S10. Comparison of XPS analysis of NiCu-SiO_2 nanocomposite before (top line) and after (bottom line) long-term recycling tests.

Table S2. Comparison of atom percentages of NiCu-SiO_2 nanocomposite before and after long-term recycling tests.

catalysts	Atom Percentages (%)		
	Ni	Cu	Si
Before catalytic	43.37	4.25	52.38
After catalytic	34.13	3.19	62.68

As the TEM image in Figure S9B shows that after 20 times successive catalytic tests NiCu NPs of NiCu-SiO_2 nanocomposite were coated by a layer of nanosheets. To confirm the composition of surface-covered nanosheets, the XPS analysis of NiCu-SiO_2 nanocomposite after tests was also measured. As shown in Figure S10 and Table S2, we can observed that Si content of the nanocomposite surface increased after long-cycling tests, meanwhile, Ni and Cu content decreased. Thus we conclude the nanosheets covered on NiCu NPs is SiO_2.

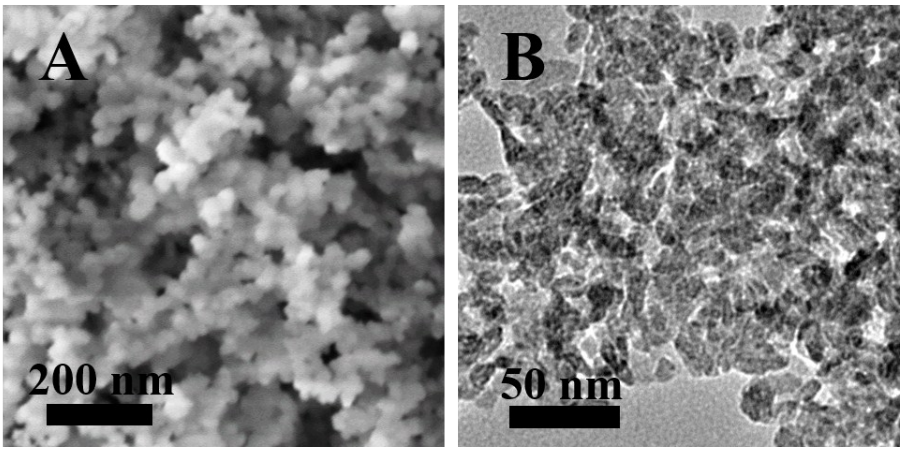

Figure S11. SEM (A) and TEM (B) images of NiCu alloy NPs after 5 times successive catalytic tests.

The morphology of NiCu alloy NPs after 5 times successive catalytic tests was also monitored and shown in Figure S11. The SEM and TEM images show a quite easy agglomeration compared with NiCu-SiO_2 nanocomposite, which eventually leads to the catalyst invalid, indicating the catalytic stability can be efficiently promoted by embedding NiCu alloy NPs in SiO_2 membrane.

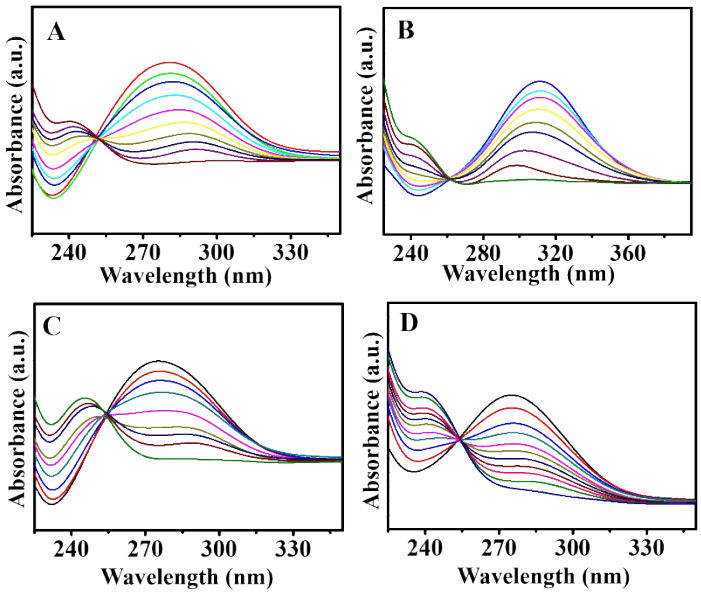

Figure S12. UV-Vis spectra of NiCu-SiO_2 nanocomposite catalyse other nitroarenes: (A) 4-nitrotoluene, (B) 4-nitroanisole, (C) 4-nitrobenzylalcohol, (D) 4-nitrobenzaldehyde.

For more comprehensively evaluating the catalytic performance of 2D structured NiCu-SiO_2 nanocatalyst, different nitroarenes have been designated as the catalytic substrates and the UV-Vis adsorption spectra were presented in Figure S12. It can be observed that most substrates can be converted completely, and the rate constants *k* of all these reactions reached a favorable level. In addition, as shown in Table 1 the selectivity are all above 90%. It revealed the excellent universality of the as-prepared 2D structured NiCu-SiO_2 nanocatalyst for the nitro-amination reaction.